Available online at www.sciencedirect.com

ScienceDirect

Geochimica et Cosmochimica Acta 231 (2018) 1–14

Geochimica et Cosmochimica Acta

www.elsevier.com/locate/gca

Distinguishing summertime atmospheric production of nitrate across the East Antarctic Ice Sheet

G. Shi [a,b,*], A.M. Buffen [c], H. Ma [b], Z. Hu [b], B. Sun [b], C. Li [d], J. Yu [b], T. Ma [b], C. An [b], S. Jiang [b], Y. Li [b], M.G. Hastings [c,*]

[a] *Key Laboratory of Geographic Information Science (Ministry of Education), School of Geographic Sciences and Institute of Eco-Chongming, East China Normal University, Shanghai 200241, China*

[b] *Polar Research Institute of China, Shanghai 200062, China*

[c] *Department of Earth, Environmental and Planetary Sciences and Institute at Brown for Environment and Society, Brown University, Providence, RI 02912, USA*

[d] *The State Key Laboratory of the Cryospheric Sciences, Northwest Institute of Eco-Environment and Resources, Chinese Academy of Sciences, Lanzhou 730000, China*

Received 28 October 2017; accepted in revised form 29 March 2018; available online 5 April 2018

Abstract

Surface snow and atmospheric samples collected along a traverse from the coast to the ice sheet summit (Dome A) are used to investigate summertime atmospheric production of nitrate (NO_3^-) across East Antarctica. The strong relationship observed between $\delta^{15}N$ and $\delta^{18}O$ of nitrate in the surface snow suggests a large (lesser) extent of nitrate photolysis in the interior (coastal) region. A linear correlation between the oxygen isotopes of nitrate ($\delta^{18}O$ and $\Delta^{17}O$) indicates mixing of various oxidants that react with NO_x ($NO_x = NO + NO_2$) to produce atmospheric nitrate. On the plateau, the isotopes of snow nitrate are best explained by local reoxidation chemistry of NO_x, possibly occurring in both condensed and gas phases. Nitrate photolysis results in redistribution of snow nitrate, and the plateau snow is a net exporter of nitrate and its precursors. Our results suggest that while snow-sourced NO_x from the plateau due to photolysis is a significant input to the nitrate budget in coastal snow (up to ~35%), tropospheric transport from mid-low latitudes dominates (~65%) coastal snow nitrate. The linear relationship of $\delta^{18}O$ vs. $\Delta^{17}O$ of the snow nitrate suggests a predominant role of hydroxyl radical (OH) and ozone (O_3) in nitrate production, although a high $\Delta^{17}O(O_3)$ is required to explain the observations. Across Antarctica the oxygen isotope composition of OH appears to be dominated by exchange with water vapor, despite the very dry environment. One of the largest uncertainties in quantifying nitrate production pathways is the limited knowledge of atmospheric oxidant isotopic compositions.

Keywords: Nitrate; Isotopes; Snow; Atmosphere; East Antarctica

1. INTRODUCTION

There is great interest in using the isotopic composition of nitrate (NO_3^-) in ice cores to track the history of atmospheric precursor (i.e., $NO_x = NO + NO_2$) sources and oxidation chemistry. However, NO_3^- can be lost from the snowpack by surface processes, and the extent of NO_3^- loss via post-depositional processing may be accumulation

* Corresponding authors at: 500 Dongchuan Rd, Key Laboratory of Geographic Information Science (Ministry of Education), School of Geographic Sciences, East China Normal University, Shanghai 200241, China (G. Shi).

E-mail addresses: gt_shi@163.com (G. Shi), meredith_hastings@brown.edu (M.G. Hastings).

https://doi.org/10.1016/j.gca.2018.03.025
0016-7037/

dependent (Freyer et al., 1996; Röthlisberger et al., 2002; Grannas et al., 2007). In addition, the physical evolution of the snow influences the chemical composition and recent modeling of the co-condensation of HNO_3 and water vapor suggests that this could influence the deposition and preservation of NO_3^- in surface snow (Bock et al., 2016). Post-depositional loss of NO_3^- can be severe at low accumulation sites such as Dome C (<30 kg m^{-2} a^{-1}) and is accompanied by isotopic modification of the residual NO_3^- (Frey et al., 2009; Erbland et al., 2013). In contrast, NO_3^- can be largely preserved under higher snow accumulation conditions such as at Summit, Greenland (>200 kg m^{-2} a^{-1}) likely owing to the faster burial and possibly snow impurity content (Hastings et al., 2005; Fibiger et al., 2013; Zatko et al., 2013). Thus, it has been suggested that high-accumulation sites with less post-depositional processing have great potential to deliver information regarding NO_x sources and oxidation chemistry (Hastings et al., 2009; Erbland et al., 2013; Shi et al., 2015; Zatko et al., 2016). For lower accumulation sites, it can be difficult to interpret archived records due to surface modification, although the isotopic composition of NO_3^- may be useful in this regard since post-depositional loss leaves a large isotopic imprint (Erbland et al., 2015).

A number of field observations and laboratory experiments suggest that photolysis is the dominant NO_3^- loss mechanism and leads to a large enrichment of ^{15}N in the remaining snow NO_3^-, with local impacts on summertime atmospheric NO_x/OH mixing ratios via photoproducts (e.g., NO_2) (Davis et al., 2004; Jacobi et al., 2006; McCabe et al., 2007; Davis et al., 2008; Frey et al., 2009; Slusher et al., 2010; Erbland et al., 2013; Berhanu et al., 2014). Due to photolytic loss, isotopic enrichment in ^{18}O and ^{17}O of the residual snow NO_3^- is also expected (Frey et al., 2009), but field and laboratory studies tend to show a decrease in $\delta^{18}O$ and $\Delta^{17}O$ (McCabe et al., 2005; Shi et al., 2015). (δ (“delta”) is defined as $(R_{sample}/R_{reference} - 1) \times 1000‰$, where $R = {}^{15}N/{}^{14}N$ for $\delta^{15}N$, $R = {}^{18}O/{}^{16}O$ for $\delta^{18}O$ and $R = {}^{17}O/{}^{16}O$ for $\delta^{17}O$; $\Delta^{17}O = \delta^{17}O - 0.52 \times \delta^{18}O$; and the reference is air-N_2 for $\delta^{15}N$ and Vienna Standard Mean Ocean Water (VSMOW) for $\delta^{17}O$ and $\delta^{18}O$). McCabe et al. (2005) determined in laboratory photolysis experiments that the decrease in $\Delta^{17}O$ of NO_3^- in water was due to reoxidation and O-exchange reactions between the photoproducts, OH and H_2O ($\Delta^{17}O(H_2O) = 0‰$).

Photoproducts from photolysis of NO_3^- in snow can be reoxidized and recycled in the atmosphere before local re-deposition as NO_3^- or transport away. Observations in coastal regions of Antarctica have suggested that snow-sourced NO_3^-/NO_x from photolysis on the Antarctic plateau could be transported and deposited in the coastal zone (Davis et al., 2004; Savarino et al., 2007; Davis et al., 2008; Slusher et al., 2010; Grilli et al., 2013). Model simulations have suggested that most of the NO_3^- in inland Antarctic snow is lost via photolysis (perhaps greater than 90%), leading to a large enrichment of ice core $\delta^{15}N$ of NO_3^- (up to 300–400‰), while the recycled NO_3^- due to transported photoproducts contributes to a lowering of $\delta^{15}N$ in coastal snow (Zatko et al., 2016). However, another modeling study concluded that tropospheric sources of NO_x from mid-latitudes (i.e., fossil fuel combustion, soil, lightning, and thermal decomposition of peroxyacetylnitrate (PAN)) are the main driver of NO_3^- concentrations in snow except in summer (Lee et al., 2014). This latter modeling study did not include photolytic loss or recycling of snow NO_3^- and suggested that observed summertime peaks (November–January) in snow NO_3^- concentrations across Antarctica would likely be explained if this process were included. Previous observational studies had suggested that a stratospheric source of NO_3^- was an important driver of seasonality in NO_3^- concentrations in spring and early summer (Legrand and Delmas, 1986; Wagenbach et al., 1998; Savarino et al., 2007; Traversi et al., 2017). The potential mix of tropospheric and stratospheric sources, and the atmospheric transport of ‘secondary’ NO_3^-/NO_x across the East Antarctic Ice Sheet (EAIS) adds additional complexity to the interpretation of NO_3^- in ice cores.

In an effort to better discern the influence of production of ‘secondary’ NO_3^- in Antarctica, we collected surface snow and atmospheric samples along a ~1300 km traverse from coastal East Antarctica to the summit of the ice sheet (Dome A). This traverse covers a variety of environments, e.g., from very low (<25 kg m^{-2} a^{-1}) to high (>200 kg m^{-2} a^{-1}) snow accumulation rates, from the coast to the ice sheet summit (with elevation ~4100 m). We utilize the full suite of NO_3^- isotopic measurements ($\delta^{15}N$, $\delta^{18}O$ and $\Delta^{17}O$) on snow and atmospheric samples to investigate processing of snow NO_3^- and formation pathways of atmospheric NO_3^- in different environments on the EAIS.

2. METHODOLOGY

2.1. Sample collection

In austral summer 2012–2013, surface snow samples were collected from 124 sites at ~10 km intervals along a traverse from Zhongshan Station on the coast to Kunlun Station at Dome A (Fig. 1). The topmost 3 ± 1 cm of snow was collected using 250 ml high-density polyethylene (HDPE) bottles pushed into the snow in the windward direction. The surface snow sampling was carried out upwind with respect to the traverse route, generally >500 m away from the route. The bottles were pre-cleaned with ultrapure Milli-Q water (18.2 MΩ), dried under a class 100 clean hood at room temperature and sealed in clean polyethylene (PE) bags until field sampling. Pre-cleaned bottles filled with Milli-Q water taken to the field and treated to the same conditions as samples represent field blanks. After sampling, the bottles were again sealed in clean PE bags and preserved frozen in a clean insulated cabinet. At individual sampling sites, the surface snow density (the topmost ~10 cm layer) was measured using a rectangular sampler (total volume = 1000 cm^3).

In addition to surface snow, atmospheric NO_3^-, i.e., both particulate and gaseous NO_3^-, was collected along the traverse following similar protocols for previous work in East Antarctica (Savarino et al., 2007; Frey et al., 2009; Erbland et al., 2013). Briefly, the atmospheric samples were collected on Whatman G653 glass-fiber filters (8 × 10 in; prebaked at

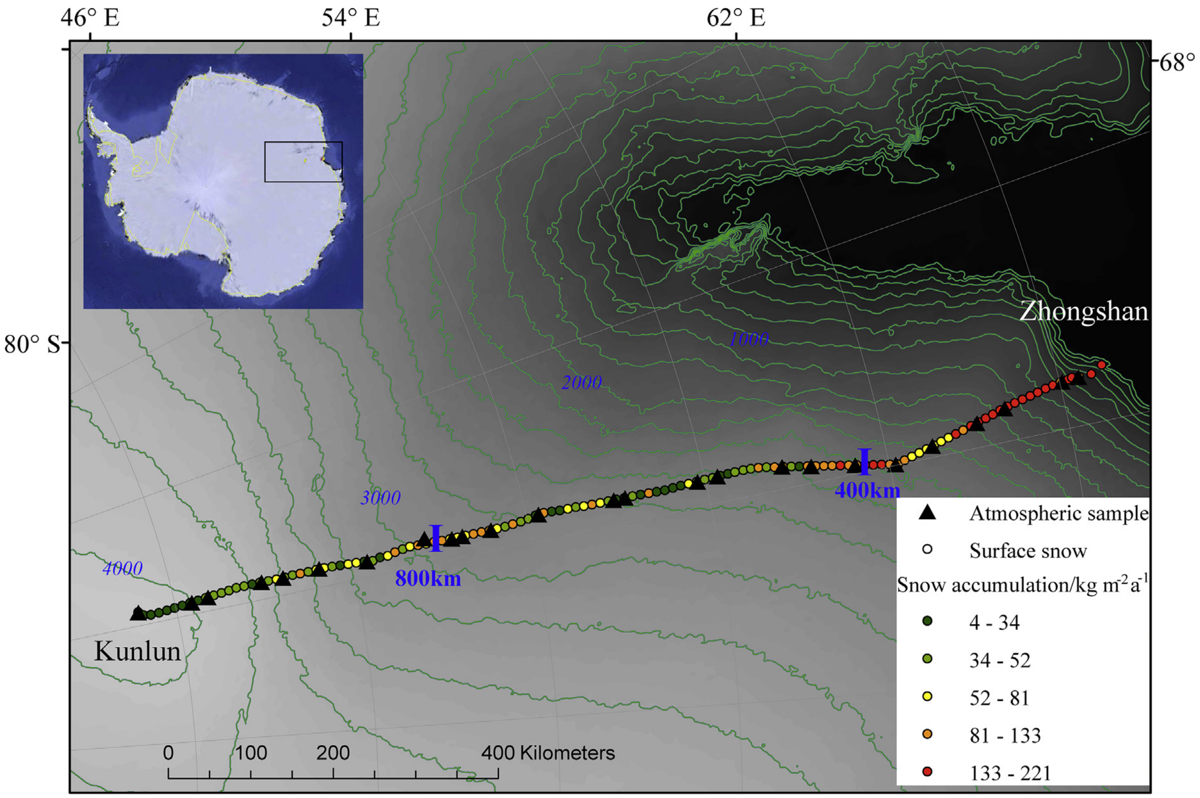

Fig. 1. Surface snow and atmospheric nitrate sampling sites along the traverse from coast (Zhongshan Station) to Dome A (Kunlun Station), East Antarctica. The surface snow and atmospheric nitrate sampling sites are denoted by circles and closed triangles, respectively. Note that the different color of the closed circles corresponds to the varied annual snow accumulation rate on the traverse (in kg m^{-2} a^{-1}), which was obtained by measuring surface mass balance stakes between 2009 and 2013, and the details of this stick measurement were reported in Ding et al. (2011). The annual snow accumulation rate on the traverse is also shown in Fig. 2(a).

550 °C for ~24 h) using a high volume air sampler (HVAS), with a flow rate of ~1.0 m^3 min^{-1} for 12–15 h. All sampling was performed ~200 m upwind from the temporary field camps. Two HVASs were operated at the same time to ensure sufficient amounts of NO_3^- for isotopic analysis, and the two filters were combined to form one sample. In total, 34 atmospheric samples were collected on the traverse (Fig. 1).

Recent model simulations suggest that the tropospheric transport of NO_x emitted as far north as 25°S is an important contribution to the Antarctic NO_3^- budget (Lee et al., 2014), and characterizing the isotopic signatures of NO_3^- in the southern mid-low latitudes would be of significance to the interpretation of NO_3^- sources in Antarctic snow. Thus, marine atmospheric NO_3^- was sampled in the Indian Ocean sector by the RV Xuelong during the 2015–2016 Chinese Antarctic Expedition cruise (Table S1). The sampling protocols were similar to those described here. To avoid contamination from the vessel's emissions, the HVAS was situated on the top deck (~25 m above sea level) and operated only when the incoming wind direction was perpendicular to the vessel's path and the wind velocity was greater than 1.5 m s^{-1}. The sampling durations were 24–48 h, with the typical sampling air volume for each sample ranging from about 1500 to 3500 m^3. In total, 10 atmospheric samples in the mid-low latitudes (~20–45 °S) were collected. (We note that samples were collected along the entire cruise route and the full dataset is the subject of a forthcoming publication.) Four field blanks were collected from filters installed in the HVAS without pumping and treated as samples thereafter. All filters were kept in opaque PE bags before and after collection and stored at <−20 °C prior to extraction and analysis.

2.2. Sample analysis

The procedure for extracting filter NO_3^- was similar to previous work (Xu et al., 2013). Each filter was cut into pieces using pre-cleaned scissors that were rinsed between samples, placed in ~ 100 ml of Milli-Q water, ultrasonicated for 40 min and leached for 24 h under shaking. The sample solutions were then filtered through 0.22 μm ANPEL PTFE filters for NO_3^- concentration and isotopic analysis. Nitrate concentration ($[NO_3^-]$) in snow and extracted solutions was determined using a Dionex ion chromatograph (ICS 3000) following Shi et al. (2012). The pooled standard deviation ($1\sigma_p$; Table S2) of replicate samples run at least twice in different sample sets was 1.5 ng g^{-1} ($n = 25$). The detection limit (DL) of NO_3^- is obtained from three standard deviations of Milli-Q water in the lab, which is typically run 10 times, and the DL is estimated to be ~3.0 ng g^{-1}. $[NO_3^-]$ in the field blanks

($n = 3$) consisting of bottled Milli-Q water taken to Antarctica was near or below detection limit. For the glass fiber filter blanks ($n = 4$), [NO_3^-] was generally two orders of magnitude lower than actual atmospheric sample extract solutions (hundreds to thousands of ng ml^{-1}).

Water oxygen isotope ratios ($\delta^{18}O(H_2O)$) of snow were determined by a Finnigan MAT253 isotope ratio mass spectrometer (IRMS) using the standard CO_2 equilibration method (Johnsen et al., 1997). The $1\sigma_p$ of reference material (VSMOW) measurements was 0.10‰ ($n = 20$).

Nitrogen and oxygen isotopic ratios in NO_3^- ($\delta^{15}N$, $\delta^{18}O$ and $\Delta^{17}O$) were analyzed using the bacterial denitrifier method at Brown University (Sigman et al., 2001; Casciotti et al., 2002; Kaiser et al., 2007). Briefly, denitrifying bacteria (*Pseudomonas aureofaciens*) lacking the N_2O reductase enzyme quantitatively convert NO_3^- to $N_2O_{(g)}$ which is then analyzed for $\delta^{15}N$ and $\delta^{18}O$ using a Thermo Scientific Delta V + IRMS. $\Delta^{17}O$ was measured separately via the thermal decomposition of N_2O to N_2 and O_2 in a heated gold tube (Kaiser et al., 2007). It is noted that $\delta^{18}O$ and $\Delta^{17}O$ of NO_3^- were determined independently at Brown, i.e., different aliquots of a sample are measured separately for $\delta^{18}O$ (using N_2O) and $\Delta^{17}O$ (using O_2 decomposed from N_2O; Fibiger et al., 2013). Additional details on the isotopic measurements are described in Shi et al. (2015). The $1\sigma_p$ of sample replicates depicts the analytical precision of the overall method (Fibiger et al., 2013; Buffen et al., 2014; Shi et al., 2015), and for this work was $\delta^{15}N = 0.3‰$ ($n = 18$), $\delta^{18}O = 0.5‰$ ($n = 18$) and $\Delta^{17}O = 0.6‰$ ($n = 23$) (Table S2).

3. RESULTS

3.1. Concentration and isotopic composition of NO_3^-

The concentration and isotopic composition of NO_3^- in the snow and atmosphere are shown in Fig. 2. Snow [NO_3^-] ranges from 30.0 to 488 ng g^{-1} (mean = 51.1 ng g^{-1}) with a coefficient of variation (*Cv*, standard deviation/mean) of 0.5, indicating moderate variability. In general, [NO_3^-] in snow is comparable to other Antarctic traverses such as Dumont d'Urville (DDU)-Dome C, Talos Dome-Dome C, and Syowa-Dome F (Traversi et al., 2004; Bertler et al., 2005; Frey et al., 2009). Atmospheric [NO_3^-] varies between 6 and 118 ng m^{-3}, with a mean of 38 ng m^{-3} (Fig. 2c).

Due to the wide range of accumulation rates (which are influenced by wind scouring and redistribution in addition to precipitation), the 3 cm of snow sampled at each site covers different periods of time. At inland sites (low accumulation; Fig. 2a), very high NO_3^- concentrations have been observed in the uppermost ~1 cm of snow during austral summertime (concentrations at Dome C, for example, have been observed above 1000 ng g^{-1} (Udisti et al., 2004; Erbland et al., 2013), so we expect that the NO_3^- in our inland samples contains a significant or even dominant amount from this upper, and presumably more recent, deposition.

Snow $\delta^{15}N(NO_3^-)$ ranges from –33.6 to 110.6‰ (mean = 14.7‰; Fig. 2d), and $\delta^{18}O(NO_3^-)$ varies between 39.5 and 100.7‰ (mean = 76.3‰; Fig. 2e). *Cv* of $\delta^{18}O(NO_3^-)$ is 0.17, while *Cv* = 2.4 for $\delta^{15}N(NO_3^-)$, suggesting larger spatial variability of the latter. It is difficult to directly compare the observations here with previous isotopic data from the DDU-Dome C traverse, primarily due to difference in sampling depth. Frey et al. (2009) reported that $\delta^{15}N$ and $\delta^{18}O$ of NO_3^- in the top 10 cm of snow along the DDU-Dome C traverse was −13.3 to 36.8‰ (mean = 8.2‰) and 62.5–85.7‰ (mean = 70.6‰), respectively. These ranges are generally smaller compared to our data, possibly related to the deeper surface snow sampling in that study, while shallower surface sampling on a later DDU-Dome C traverse suggests a larger range than found here. Erbland et al. (2013) report data from 19 locations sampled at ~2 cm depth along the DDU-Dome C traverse, with $\delta^{15}N$ ranging between −31 and 186‰ (mean of 41‰). For these same samples, $\delta^{18}O$ varies between 28 and 107‰ (mean = 63‰). It is likely that significant deposition to the near surface layer of snow influences the concentration and isotopic results (see above). In the atmosphere, the ranges of $\delta^{15}N(NO_3^-)$ and $\delta^{18}O(NO_3^-)$ are −46.9 to 12.6‰ (mean = −20.1‰; Fig. 2d) and 58.7–82.7‰ (mean = 71.2‰; Fig. 2e), respectively, and these values generally fall within the ranges measured at Dome C and DDU (Savarino et al., 2007; Erbland et al., 2013).

Snow $\Delta^{17}O(NO_3^-)$ ranges from 23.7 to 36.5‰, with a mean of 31.1‰ and *Cv* of 0.07 (Fig. 2f), showing much less spatial variability than either $\delta^{15}N(NO_3^-)$ or $\delta^{18}O(NO_3^-)$. Information regarding $\Delta^{17}O(NO_3^-)$ in Antarctic surface snow is rather limited but data from a DDU-Dome C traverse range from 27 to 38‰ (Erbland et al., 2013). Atmospheric $\Delta^{17}O(NO_3^-)$ ranges from 24.0 to 30.1‰, with a mean of 27.7‰. Similar to $\delta^{15}N(NO_3^-)$ and $\delta^{18}O(NO_3^-)$, $\Delta^{17}O(NO_3^-)$ here is comparable to the austral summer observations at Dome C and DDU (Savarino et al., 2007; Erbland et al., 2013). Note that previous works on isotopes of atmospheric NO_3^- are site-specific observations (i.e., focusing on temporal/seasonal variations; Wagenbach et al., 1998; Savarino et al., 2007; Erbland et al., 2013), and data on the spatial variation across Antarctica (e.g., spatial variability along a traverse) are unavailable thus far.

Atmospheric [NO_3^-] in the marine boundary layer in the southern mid-low latitudes (from about 20°S to 45°S) ranges from 50 to 1350 ng m^{-3}, which is similar to the previous investigations along the same cruise (Xu et al., 2013; Xu and Gao, 2015). Means of $\delta^{15}N$, $\delta^{18}O$ and $\Delta^{17}O$ of atmospheric NO_3^- are -7.0 ± 3.7, 70.7 ± 8.2 and 25.1 ± 2.6‰ (mean ± 1σ, $n = 10$), respectively (Table S1), comparable to the observations in the Atlantic Ocean over the same latitudinal range (Morin et al., 2009).

3.2. NO_3^- concentration and isotopic composition spatial pattern

In general, both [NO_3^-] and $\delta^{15}N$ in the snow and atmosphere increase from the coast towards the plateau while $\delta^{18}O$ shows an opposite trend, with lower values inland (Fig. 2c–e). This is similar to surface snow observations along the DDU-Dome C traverse (Frey et al., 2009). $\Delta^{17}O$ shows a generally similar but much weaker trend as with $\delta^{18}O$ (Fig. 2e and f).

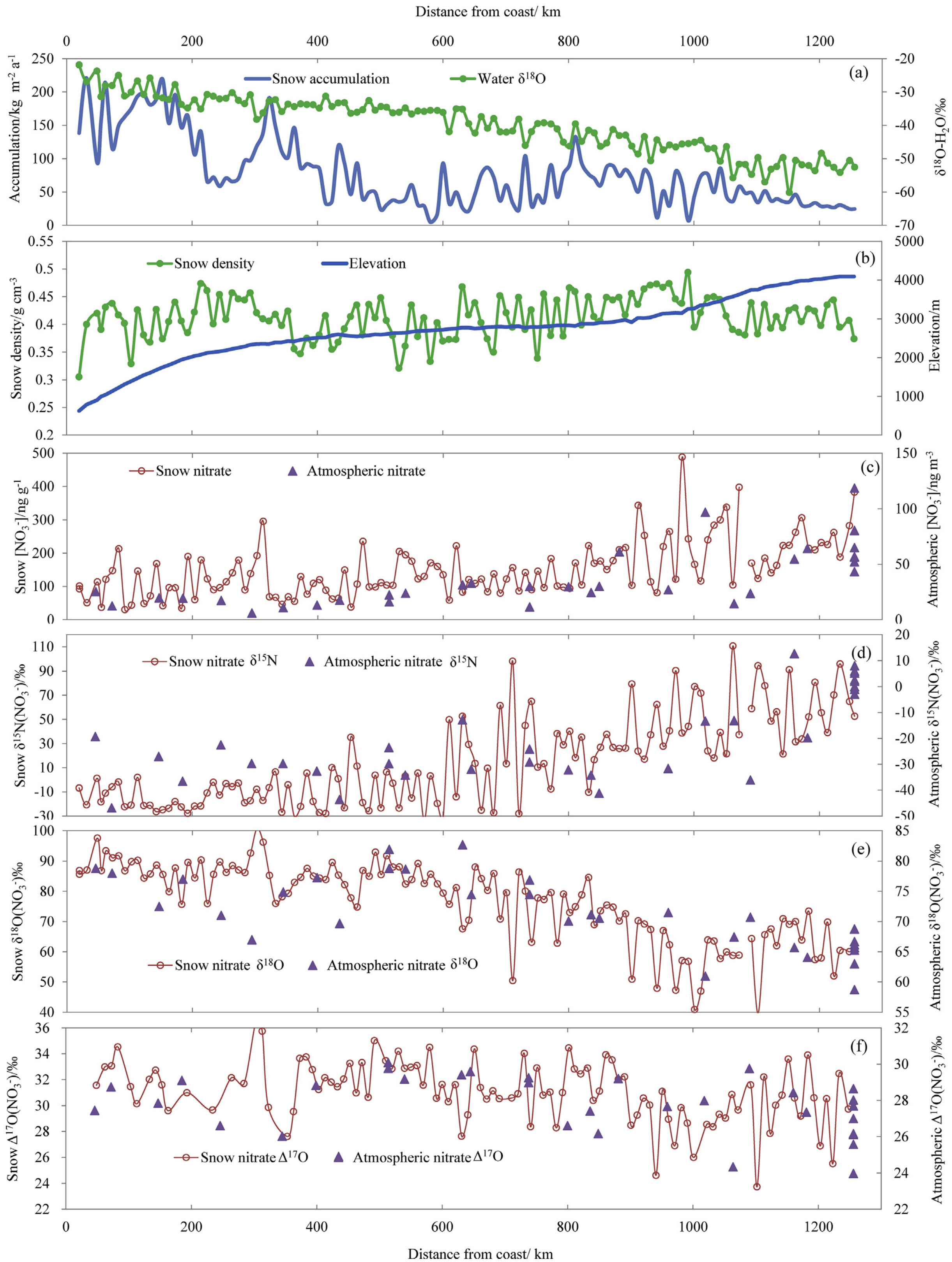

Fig. 2. Annual snow accumulation rate and water isotopes (a), and snow density and elevation (b), along the traverse from Zhongshan Station to Dome A, East Antarctica. Results for concentration and isotopic composition of NO_3^- ((c)–(f)) in surface snow and atmosphere. Note that the atmospheric data of $\delta^{15}N$, $\delta^{18}O$ and $\Delta^{17}O$ on the secondary *y*-axis are presented with a different scale from the primary *y*-axis (snow NO_3^- isotopic data) ((d)–(f)).

A significant correlation was found between $\delta^{18}O$ and $\delta^{15}N$ of NO_3^- in the snow and atmosphere (Fig. 3), while $\delta^{18}O$ and $\Delta^{17}O$ of NO_3^- are closely related in snow (Fig. 4). However, the concentration generally shows no relation to the isotopic parameters of NO_3^- in snow, except the data on the plateau (i.e., 800 km – Dome A), where positive correlations were found between oxygen isotopes ($\delta^{18}O$ and $\Delta^{17}O$) and concentration ($R^2 = 0.31$ and 0.41, respectively; Fig. S1). In the atmosphere, $[NO_3^-]$ is well correlated with $\delta^{18}O$ or $\delta^{15}N$, but not with $\Delta^{17}O$ (Fig. S2).

Both $\delta^{15}N$ and $\delta^{18}O$ in the snow NO_3^- are most strongly, and non-linearly, related to site distance from the coast and elevation (since elevation increases inland; Table 1). The same is true for $[NO_3^-]$ and $\Delta^{17}O$ but to a lesser degree. Interestingly, there are no significant trends from the coast to ~400 km inland for snow NO_3^- isotopic compositions ($R^2 < 0.1$, $p > 0.05$; Figs. S3 and S4). In the coastal ~400 km, the snow accumulation rate is high, generally >100 kg m^{-2} a^{-1} (Fig. 2a), which may restrict the post-depositional alteration of snow NO_3^-, leading to no clear trend in isotopic composition (see Section 4.2 below).

Previous reports have pointed out that snow $[NO_3^-]$ and/or isotopic composition across Antarctica are related to site accumulation rate (Freyer et al., 1996; Röthlisberger et al., 2002; Erbland et al., 2013). The weak relationships with accumulation observed in this work are likely related to the very strong wind scouring and snow redistribution that results in low measured accumulation at mid-traverse sites (covering about 400–800 km) (Das et al., 2013), as opposed to low accumulation due to low precipitation as is the case on the plateau (Ding et al., 2011) (Fig. S5). When sites from the mid-traverse are not considered, the relationships with accumulation improve but do not exceed those with distance from the coast (Tables 1 and S3). We note that when these mid-traverse sites are not considered, there is very little change in the relationships among $\delta^{15}N$, $\delta^{18}O$, $\Delta^{17}O$ and $[NO_3^-]$. In the following, the transition zone is excluded such that only the plateau (~800 km – Dome A, with snow accumulation decrease towards Dome A and elevation >~3000 m) and coastal (coast – ~400 km) sites will be focused on.

4. DISCUSSIONS

4.1. Plateau snow NO_3^-: post-depositional processing and recycling

If it is assumed that photolytic loss of snow NO_3^- follows a Rayleigh type process, a theoretical fractionation constant, ε (‰), can be used to quantify the changes in $\delta^{15}N$ or $\delta^{18}O$ with NO_3^- processing (Blunier et al., 2005). Under the summertime radiation conditions on the Dome A plateau, the $^{15}\varepsilon$ (^{15}N) and $^{18}\varepsilon$ (^{18}O) are calculated to be −53‰ and −34‰ respectively, following the model proposed by Frey et al. (2009). This negative $^{15}\varepsilon$ value, close to that derived from both laboratory and field experiments (Berhanu et al., 2014, 2015), would explain the inland high snow $\delta^{15}N(NO_3^-)$, with larger values corresponding to a higher degree of photolytic loss of NO_3^- (Fig. 3a). Consequently, higher atmospheric $[NO_3^-]$ values are observed on the plateau due to the strong photolytic loss of snow NO_3^- (Fig. 2c), and the atmospheric NO_3^- is expected to hold the isotopic imprint of snow-sourced NO_3^- (i.e., secondary NO_3^- from snow-sourced NO_x).

Upon photolysis of NO_3^-, the $\delta^{15}N$ of emitted NO_x can be calculated following the Rayleigh fractionation equation,

$$\delta^{15}N_{emitted} = (1+\delta^{15}N_0)(1-f^{(^{15}\varepsilon+1)})/(1-f) - 1, \qquad (1)$$

where $\delta^{15}N_0$ denotes $\delta^{15}N$ in initially deposited NO_3^-; f is the fraction of NO_3^- remaining in the snow. If we take $\delta^{15}N$ in initially deposited NO_3^- at Dome A to be similar to that at Dome C (i.e., $\delta^{15}N_0 = 18‰$, top ~0.4 cm snow value; Erbland et al., 2013) and $f = 0.63$ (i.e., a ~37% loss of NO_3^- in inland Antarctica; Shi et al., 2018), the $\delta^{15}N_{emitted}$ is calculated to be ~−26‰, i.e., very negative $\delta^{15}N(NO_x)$ values would be expected in the atmosphere above the plateau snowpack. Assuming that secondary $\delta^{15}N(NO_3^-) \approx$

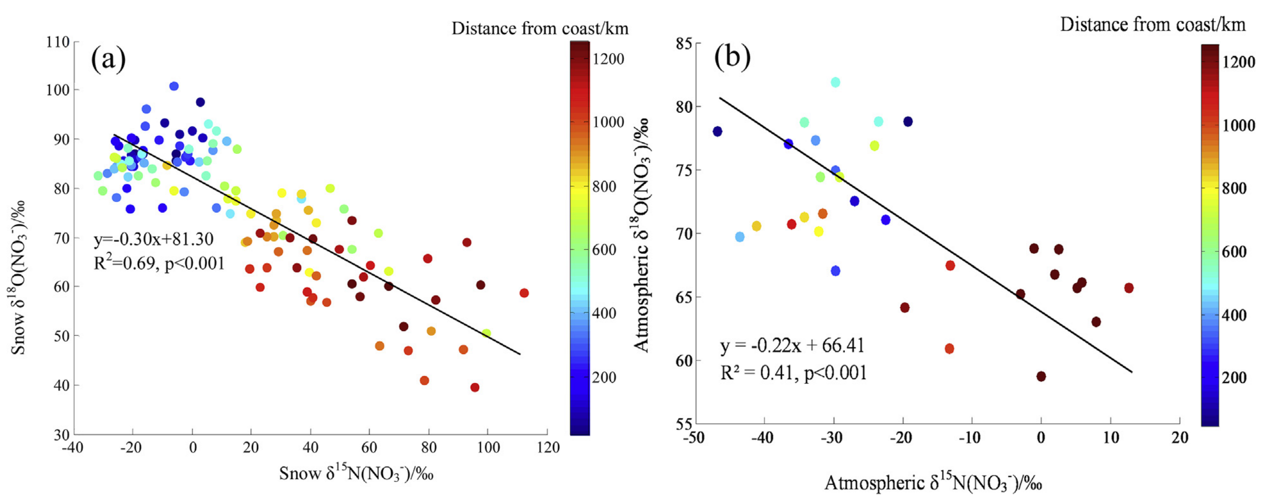

Fig. 3. Relationship between $\delta^{15}N$ and $\delta^{18}O$ of NO_3^- in the snow (a) and atmosphere (b), with colors corresponding to site distance from the coast.

Table 1
Coefficient of determinations (R^2) for best-fit regressions of snow NO_3^- concentration and isotopic composition vs. distance from coast, elevation (m above sea level; m a.s.l.), snow accumulation rate and inverse accumulation rate. The best non-linear fit type was shown after the R^2.

Parameter	$[NO_3^-]$, ng g^{-1}	$\delta^{15}N(NO_3^-)$, ‰	$\delta^{18}O(NO_3^-)$, ‰	$\Delta^{17}O(NO_3^-)$, ‰
Distance from coast, km	0.38*, P[a]	0.62*, P	0.67*, P	0.22*, P
Elevation, m a.s.l.	0.33*, P	0.57*, P	0.64*, P	0.20*, P
Snow accumulation rate, kg m^{-2} a^{-1}	0.13, Exp[b]	0.27*, P	0.25*, P	0.11, P
1/Accumulation	0.12, Pow[c]	0.30*, P	0.25*, P	0.09, P

[a] P, polynomial.
[b] Exp, exponential.
[c] Pow, power.
* Significant at $p < 0.05$.

$\delta^{15}N(NO_x)$, the observed atmospheric $\delta^{15}N(NO_3^-)$ is much higher than the expected values from a Rayleigh fractionation for almost all of the plateau, with even positive values (>5‰) observed (Fig. 2d). These values are similar to the summer atmospheric observations at Dome C (Erbland et al., 2013).

Could another source, such as tropospheric inputs, explain this deviation from expectation? For instance, Lee et al. (2014)'s adjoint modeling study suggests tropospheric sources from the mid-low latitudes should be important. The tropospheric $\delta^{15}N(NO_3^-)$ observed in samples collected in mid-low latitudes of the Indian Ocean sector in this study was found to be negative (-7.0 ± 3.7‰), while the data in mid-low latitudes in the Atlantic Ocean sector is about −4‰ (Morin et al., 2009). Although the potential fractionation of ^{15}N during transport is not well understood, it is unlikely that the tropospheric source contributes substantially to positive atmospheric $\delta^{15}N(NO_3^-)$ on the plateau rather than on the coast (i.e., very low atmospheric $\delta^{15}N(NO_3^-)$ on the coast; Fig. 2d). Stratospheric inputs of NO_3^- have also been hypothesized as important on the plateau, and this source is expected to have a high, positive $\delta^{15}N(NO_3^-)$ value (19 ± 3‰) (Moore, 1974; Savarino et al., 2007). A stratospheric source of NO_3^-, however, should also have a high $\delta^{18}O$ and $\Delta^{17}O$ of NO_3^- due to the influence of stratospheric ozone (Krankowsky et al., 2007) and this is opposite to the observations (Figs. 3 and 4).

This brings us back to the possibility that the recycling of NO_3^- on the plateau dominates the atmospheric NO_3^- pool. In the campaigns of Investigation of Sulfur Chemistry in the Antarctic Troposphere (ISCAT) and Antarctic Tropospheric Chemistry Investigation (ANTCI) at South Pole during 1990s–2000s, elevated atmospheric NO_x levels on the plateau were proposed to be associated with NO_3^- recycling (Davis et al., 2004, 2008). Recent box model and global chemical transport model simulations suggest that NO_3^- recycling at the low snow accumulation sites, e.g., Dome C, is rather strong (>4 times before burial below the photic zone) (Erbland et al., 2015; Zatko et al., 2016). During photolysis of NO_3^-, some of the photoproducts are emitted into the gas phase and can be transported away by katabatic winds, leading to a net loss of NO_3^-, and regionally, the Antarctic plateau regions are predicted to be subjected to the largest losses of NO_3^- (Zatko et al., 2016). This NO_3^- net loss process would result in a large enrichment of ^{15}N in the snow, and subsequently the atmosphere on the plateau (i.e., the increased $\delta^{15}N(NO_3^-)$ values in the surface snow due to loss then lead to positive $\delta^{15}N(NO_x)$ via photolysis). The local production of secondary NO_3^- in the atmosphere is also consistent with the oxygen isotopic composition observations (see below). It is possible that the imprint of stratospheric NO_3^- could also help explain the positive values on the plateau; however, the model studies suggest that at such sites nearly 100% of the NO_3^- should reflect a recycled signal. Thus, we propose that the observations of summertime atmospheric NO_3^- on the plateau (Figs. 2c and 3b) are best explained by the recycling of photolyzed NO_3^- products across the plateau. Accordingly, this leads to a spatial redistribution of NO_3^- driven by photochemistry that also contributes to depleted $^{15}N(NO_3^-)$ in the coastal snow (Section 4.2).

As a mass-dependent process, it is expected that photolysis alone will not change the $\Delta^{17}O$ of NO_3^- remaining in the snow, but will increase $\delta^{18}O$ following from the very negative calculated $^{18}\varepsilon = -34$‰, as is the case with $\delta^{15}N$ (Frey et al., 2009). On the plateau, the high $\delta^{15}N(NO_3^-)$ corresponds to low $\delta^{18}O(NO_3^-)$ (Fig. 3), and $\Delta^{17}O(NO_3^-)$ also shows low values (Figs. 2f and 4), opposite to the expectations. During photolysis, however, some of the photoproducts remain in the condensed phase (Jacobi and Hilker, 2007) and undergo reoxidation reactions where oxygen atoms from OH and/or H_2O (with very negative $\delta^{18}O$ and $\Delta^{17}O \approx 0$; case 1 in Table 2; Fig. 2a) can be incorporated into this secondary snow NO_3^-. In this case, both $\delta^{18}O$ and $\Delta^{17}O$ in remaining snow NO_3^- will be lowered. This is supported by laboratory and theoretical work (McCabe et al., 2005; Jacobi and Hilker, 2007) and has been invoked to explain other East Antarctic snowpit observations (Frey et al., 2009; Erbland et al., 2013; Shi et al., 2015). Simultaneously, some fraction of the photoproducts must also escape the condensed phase to the firn air and overlying atmosphere. These products should also undergo reoxidation (but in the gas phase) by local oxidants (e.g., OH; see below). This reformed NO_3^- will either be redeposited (where it may undergo further recycling) or be transported away. The combination of loss and reformation of NO_3^- can explain higher $\delta^{15}N$ corresponding to lower $\delta^{18}O$ in the snowpack at plateau sites (Fig. 3).

During the production of atmospheric NO_3^-, oxygen atoms are incorporated from different source oxidants,

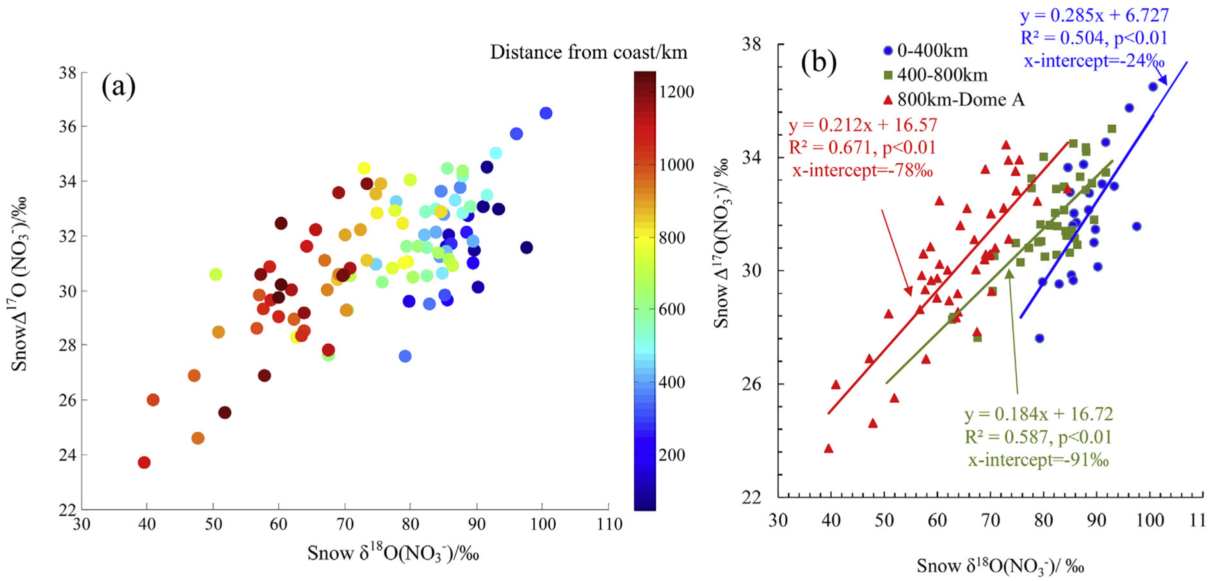

Fig. 4. Δ^{17}O vs. δ^{18}O of NO_3^- in surface snow. The relationship between δ^{18}O and Δ^{17}O of NO_3^- ($R^2 = 0.54$, $p < 0.001$) with colors corresponding to site distance from the coast is in (a). The best fit equation, coefficient of determinations (R^2), and significance level (p) for the three groups of data (based upon distance from the coast) are shown in (b). (For interpretation of the references to color in this figure legend, the reader is referred to the web version of this article.)

Table 2
Different NO_3^- production cases in both interior and coast of Antarctica.

Plateau: 800 km-Dome A	Case 1 Reoxidation by OH in condensed phase and gas phase $\delta^{18}O(O_3^*) = 130‰$, $\Delta^{17}O(O_3^*) = 39‰$; $\delta^{18}O(H_2O) = [-40.0‰, -60.2‰]$[a]; $\delta^{18}O(H_2O)_v = [-62.8‰, -86.2‰]$[b]; $\Delta^{17}O(OH) \approx 0‰$; $\Delta^{17}O(NO_2) = \alpha * \Delta^{17}O(NO_2)_{O3+NO}$[c]	Case 1A Condensed phase, $\delta^{18}O(OH) = \delta^{18}O(H_2O) = [-40.0‰, -60.2‰]$; Gas phase, $\delta^{18}O(OH) = \delta^{18}O(H_2O)_v = [-69.1‰, -81.3‰]$
		Case 1B Condensed phase, $\delta^{18}O(OH) = \delta^{18}O(H_2O) + \varepsilon_{OH\text{-}H2O}$[d] $= [-92.9‰, -114.8‰]$; Gas phase, $\delta^{18}O(OH) = \delta^{18}O(H_2O)_v + \varepsilon_{OH\text{-}H2O} = [-111.2‰, -135.3‰]$
Coast: 0–400 km	Case 2 Three NO_3^- production pathways, i.e., OH, O_3 and BrO $\delta^{18}O(O_3^*) = 130‰$, $\Delta^{17}O(O_3^*) = 39‰$; $\delta^{18}O(H_2O) = [-21.9‰, -31.0‰]$; $\delta^{18}O(H_2O)_v = [-40.0‰, -59.7‰]$; $\Delta^{17}O(H_2O)_v = 0‰$; $\Delta^{17}O(OH) = r$[e] $* (1/2\Delta^{17}O(O_3^*) + 1/2\Delta^{18}O(H_2O)_v) + (1-r) * \Delta^{18}O(H_2O)_v \approx 2.5‰$	Case 2A $\delta^{18}O(OH) = r * (1/2\delta^{18}O(O_3^*) + 1/2\delta^{18}O(H_2O)_v) + (1-r) * \delta^{18}O(H_2O)_v = [-28.9‰, -47.4‰]$
		Case 2B $\delta^{18}O(OH) = r * (1/2\delta^{18}O(O_3^*)+1/2\delta^{18}O(H_2O)_v) + (1-r) * \delta^{18}O(H_2O)_v + \varepsilon_{OH\text{-}H2O} = [-77.6‰, -95.7‰]$

[a] Values in the square brackets denote the ranges of individual parameters.

[b] $\delta^{18}O(H_2O)_v$, water vapor isotopes, estimated from the equilibrium fractionation factor for the phase transitions of water between vapor and ice (Hoffmann, 1995). The δ^{18}O of snow refers to the observations in Fig. 2a.

[c] α, partition ratio of the rate of NO_2 production via O_3 (R1) vs. the total rate of NO_2 production ((R1) and (R3)). For all the cases in this table, $\Delta^{17}O(NO_2) = \alpha * \Delta^{17}O(NO_2)_{O3+NO}$. α is estimated to be 0.86 on the East Antarctic plateaus, and $\alpha \approx 0.9$ near the coast (Kunasek et al., 2008; Morin et al., 2009; Erbland et al., 2015). $\Delta^{17}O(NO_2)_{O3+NO}$ is the Δ^{17}O of NO_2 produced via (R1) (NO + O_3), and $\Delta^{17}O(NO_2)_{O3+NO} = 37.3‰$ taking $\Delta^{17}O(O_3^*) = 39‰$ ($\Delta^{17}O(NO_2)_{O3+NO} = 1.18 \times 2/3 * \Delta^{17}O(O_3^*) + 6.6‰$ (Savarino et al., 2008).

[d] $\varepsilon_{OH\text{-}H2O}$, equilibrium fractionation between OH and H_2O proposed by Michalski et al. (2011), $\varepsilon_{OH\text{-}H2O} = 0.188\,T - 99.3$, with T = temperature (K).

[e] r is dependent upon atmospheric OH formation through pathway of $O(^1D)$ and H_2O. On coast, δ^{18}O and Δ^{17}O of OH at steady state is determined by two competing reactions: (1) isotopic exchange between OH and H_2O, $^*OH + H_2{}^{16}O \rightarrow {}^{16}OH + H_2{}^*O$, with *O denoting ^{17}O and ^{18}O; and (2) OH sink reactions with CO and CH_4 (Michalski et al., 2003; Bloss et al., 2007; Morin et al., 2007). The isotopic composition of OH can then be estimated by the reaction rates of (1) and (2), as described by Morin et al. (2007). For the coastal conditions of this study, the ratio of net loss via reaction (2) to total loss by both reactions (r) is calculated to be ~0.13.

depending on the NO_x oxidation channels, resulting in different $\Delta^{17}O$ values in the produced NO_3^- (Michalski et al., 2003; Morin et al., 2007). The $\Delta^{17}O$ value of NO_3^- produced by different pathways can be calculated by the following expression,

$$\Delta^{17}O(NO_3^-) = 2/3\Delta^{17}O(NO_2) + 1/3\Delta^{17}O(\text{Oxidant}) \quad (2)$$

Three groups of NO_3^- production pathways need to be considered for $\Delta^{17}O$(Oxidant): oxidation by OH, O_3 and BrO ((R1)–(R11)):

$$NO + O_3 \rightarrow NO_2 + O_2, \quad (R1)$$

$$NO_2 + hv \overset{O_2}{\rightarrow} NO + O_3, \quad (R2)$$

$$NO + RO_2(\text{or } HO_2) \rightarrow NO_2 + RO(\text{or } OH), \quad (R3)$$

$$NO + BrO \rightarrow NO_2 + Br, \quad (R4)$$

$$NO_2 + OH + M \rightarrow HNO_3 + M, \quad (R5)$$

$$NO_2 + BrO \rightarrow BrONO_2, \quad (R6)$$

$$BrONO_2 + H_2O + \text{surface} \rightarrow HNO_3 + HOBr, \quad (R7)$$

$$NO_2 + O_3 \rightarrow NO_3 + O_2, \quad (R8)$$

$$NO_3 + DMS \text{ or } HC \rightarrow HNO_3 + \text{products}, \quad (R9)$$

$$NO_3 + NO_2 + M \rightarrow N_2O_5 + M, \quad (R10)$$

$$N_2O_{5(g)} + H_2O_{(l)} + \text{surface} \rightarrow 2HNO_{3(aq)}, \quad (R11)$$

where RO_2 is an organic peroxy radical, M is an unreactive third body such as N_2, DMS is dimethyl sulfide, and HC is a hydrocarbon. The reaction between OH and NO_2 (R5) is dominant during the day (Antarctic summer) while the reaction of O_3 with NO_2 ((R8)–(R11)) is more important at night (Antarctic winter). NO_2 can be oxidized by BrO to form NO_3^- via hydrolysis of $BrONO_2$ ((R6), (R7)). However, the oxidation of NO_x by BrO on the Antarctic plateau has been suggested to be negligible due to the very low observed BrO levels (2–3 pptv) (Frey et al., 2015; Savarino et al., 2016). During summertime, modeling predicts that (R5) should be the most important for NO_3^- deposited in Antarctica (Lee et al., 2014).

The linear relationship between $\delta^{18}O$ and $\Delta^{17}O$ of NO_3^- is generally interpreted as the result of mixing of various oxidants that react with NO_x to produce atmospheric NO_3^- (Michalski et al., 2004; Fibiger et al., 2013). Thus, the close relationship between $\delta^{18}O$ and $\Delta^{17}O$ of NO_3^- on the plateau (Fig. 4b) is representative of a mixing between two major oxidants: a higher end-member that is assumed to be ozone (O_3^* representing transferrable terminal atom of O_3, $\delta^{18}O(O_3^*) \approx 130‰$, and $\Delta^{17}O(O_3^*) \approx 39‰$ in the troposphere; Vicars and Savarino, 2014; Savarino et al., 2016), and an oxidant with very low $\delta^{18}O$ and $\Delta^{17}O$ that is difficult to identify.

The x-intercept of the linear regression of $\delta^{18}O$ versus $\Delta^{17}O$ of NO_3^- is −78‰ (plateau data; Fig. 4b), which is comparable to those in surface snow (−93‰) and snowpits (−84‰) at South Pole (McCabe et al., 2007). Based on the secondary NO_3^- production during photolysis, the lower end-member of the mixing line could be associated with OH and/or H_2O. OH in Antarctica during summertime is mainly from the reactions between (a) NO and HO_2, and (b) $O(^1D)$ and H_2O, which will result in different oxygen isotopic compositions (Morin et al., 2007). The presence of elevated mixing ratios of NO emitted by NO_3^- photolysis in snow will favor reaction (a), which explains large concentrations of OH across the high Antarctic plateau (Chen et al., 2001; Mauldin et al., 2001; Kukui et al., 2014). Thus, atmospheric OH in inland Antarctica is more likely associated with channel (a), due to the high degree of NO_3^- photolysis. In this case, $\delta^{18}O$(OH) could be close to or lower than the value of water vapor due to equilibrium between OH and H_2O, while $\Delta^{17}O$ should be close to zero (e.g., $\Delta^{17}O$(OH) calculated to be 1–3‰ at Dome C in summer) (Morin et al., 2007; Michalski et al., 2011; Savarino et al., 2016).

The $\delta^{18}O$ of OH is largely dependent on the exchange reaction between OH and H_2O (Dubey et al., 1997), and it can be approximated that OH is in equilibrium with H_2O under most conditions. In this case, a fractionation constant of this exchange reaction, $\varepsilon_{OH\text{-}H_2O}$, as a function of temperature has been proposed (Michalski et al., 2011). On the Antarctic plateau, where water vapor is at ppmv levels and OH is at <pptv levels (Kukui et al., 2014; Casado et al., 2016), it is unclear that this equilibrium fractionation would apply. There are no direct observations of $\delta^{18}O$(OH), but we may draw conclusions about its expected isotopic composition based upon the combined $\delta^{18}O$ and $\Delta^{17}O(NO_3^-)$ observations here. If we take $\delta^{18}O$ (OH) as close to that of H_2O (water vapor) in the condensed phase (gas phase) (case 1A, Table 2), the range of $\delta^{18}O$(OH) seems to explain the observations well (i.e., x-intercept = −78‰; Fig. 4b). Note that the estimated $\delta^{18}O$ of water vapor on the plateau (−62.8 to −86.2‰; Table 2) is comparable to the observations at Dome C in summertime (Casado et al., 2016), where the $\delta^{18}O$ of snow/ice is comparable to those of Dome A (Hou et al., 2009 and references therein). However, the OH pathway ((R1), (R5)) would lead to an expected $\Delta^{17}O(NO_3^-) \leq 26‰$ (case 1, Table 2), lower than most of $\Delta^{17}O(NO_3^-)$ values ($30 \pm 2‰$, mean $\pm 1\sigma$) in the plateau snow (Fig. 2f). In this case, a higher primary $\Delta^{17}O(NO_3^-)$, i.e., a higher $\Delta^{17}O(O_3^*)$ is required to account for the observed values. If the observed $\Delta^{17}O(NO_3^-)$ is mainly associated with O_3 ((R1), (R5)), then $\Delta^{17}O(O_3^*)$ of 58‰ (for calculation details see Table 2), corresponding to $\Delta^{17}O = 38‰$ of bulk O_3, is required to account for the observed $\Delta^{17}O(NO_3^-) = 30‰$. Note that this expected $\Delta^{17}O(O_3^*)$ represents an upper limit, calculated by assuming $\Delta^{17}O(OH) \approx 0‰$ (OH may retain the ozone $\Delta^{17}O$ signature) and no NO_3^- production pathway via BrO (the $\Delta^{17}O$ signature of NO_3^- produced via BrO pathway is identical to that of O_3 channel; (R1) and (R6)). This calculated $\Delta^{17}O$ of bulk O_3 is greater than suggested by observations using a nitrite coated filter technique at Dome C ($\Delta^{17}O(O_3)_{bulk} = 24.9‰$; Savarino et al., 2016), but falls within the ranges from laboratory experiments (Mauersberger et al., 2003; Michalski et al., 2014).

If OH is in equilibrium with H_2O, and an equilibrium fractionation ($\varepsilon_{OH\text{-}H_2O}$) between them (Michalski et al., 2011) is considered (case 1B, Table 2), the $\delta^{18}O$(OH) range is too negative to fit the x-intercept (−78‰). Thus, a large equilibrium fractionation between OH and H_2O cannot account for our observed data.

In summary, although the fractionation between OH and H_2O in the polar regions is poorly understood, our observations are best explained by $\delta^{18}O(OH) \approx \delta^{18}O(H_2O)_v$. Thus, it can be inferred that the isotopic composition of OH appears to be dominated by exchange with water vapor across the plateau, despite the very dry environment, and a large fractionation between OH and H_2O (or water vapor) does not seem to occur.

4.2. Coastal snow NO_3^-: sources and oxidant chemistry

Compared to interior snow, photolytic loss of NO_3^- likely occurs to a lesser extent near the coast (Zatko et al., 2016), possibly due to the faster burial of NO_3^- below the photochemically active zone as a result of higher snow accumulation rate (Fig. 2a). The lesser extent of NO_3^- photolysis seems to account for the coastal data extending towards the lower (higher) extreme for $\delta^{15}N$ ($\delta^{18}O$) of NO_3^- (Fig. 3). Thus, information on the primary deposition of NO_3^- (e.g., sources of NO_3^-) is likely preserved in the coastal snow, consistent with the snowpit observations on this traverse (Shi et al., 2015). This deduction also agrees well with the results of Dronning Maud Land and the traverse from Northern Victoria Land to Dome C, where the post-depositional losses of NO_3^- were found to be insignificant at sites with snow accumulation rates >~100 kg m^{-2} a^{-1} (Weller et al., 2004; Traversi et al., 2012).

On the coast, NO_3^- is featured with negative $\delta^{15}N(NO_3^-)$ values, with means in the snow and atmosphere of −13.7‰ and −30.6‰ respectively (Fig. 2d). These very negative values are generally lower than that attributed to most NO_x sources except microbial production in soils (Yu and Elliott, 2017; and references therein), but the contribution of this source to Antarctica has been simulated to be minor (Lee et al., 2014). While lightning should be an important natural source of NO_x in the troposphere (Murray et al., 2012; Lee et al., 2014), laboratory experiments suggested a $\delta^{15}N$ of NO_x of around 0‰ (Hoering, 1960). Stratospheric NO_y (sum of reactive nitrogen compounds) has been suggested to have a positive $\delta^{15}N$ (Savarino et al., 2007). Thus, it is hard to attribute the very low $\delta^{15}N(NO_3^-)$ values (<−20‰) to the known mid-low latitude NO_x sources (atmospheric $\delta^{15}N(NO_3^-)$ in the mid-low latitudes is ~−7.0‰; Section 3.1), although our knowledge of transport effects is very limited. Considering the large fractionation during photolysis ($^{15}\varepsilon = -53‰$), the very negative $\delta^{15}N(NO_3^-)$ is most likely associated with NO_3^- that is reformed from photoproducts from inland Antarctica carrying very low $\delta^{15}N$ (see Section 4.1). This NO_3^- source has also been proposed to be responsible for the depleted ^{15}N of atmospheric NO_3^- at DDU in summertime (Savarino et al., 2007).

Previous model simulations suggested that the primary source of NO_3^- to Antarctica is tropospheric transport (Lee et al., 2014), and the recycled NO_3^- is predicted to account for less of the annual NO_3^- deposition flux along the Antarctic coast (Frey et al., 2009; Zatko et al., 2016). The coastal dataset here provides observations to test these hypotheses, if the information on the primary deposition of NO_3^- is largely preserved. If it is assumed that the recycled NO_3^- and tropospheric transport of NO_3^- from mid-low latitudes dominate the NO_3^- flux in coastal snow, the contribution from both sources can be estimated by isotopic mass balance:

$$\delta^{15}N(NO_3^-)_{snow} = f_R\delta^{15}N(NO_3^-)_R + (1 - f_R)\delta^{15}N(NO_3^-)_T \quad (3)$$

with $\delta^{15}N(NO_3^-)_R$ and $\delta^{15}N(NO_3^-)_T$ representing $\delta^{15}N$ of recycled NO_3^- and tropospheric NO_3^- from mid-low latitude sources, respectively, and f_R of NO_3^- the fraction from recycled NO_3^-. If we assume that transport does not modify the isotopes markedly, we can roughly estimate f_R via: $\delta^{15}N(NO_3^-)_R$ is similar to the predictions from Eq. (1), $\delta^{15}N(NO_3^-)_T = -7.0‰$ from observations, and $\delta^{15}N(NO_3^-) = -13.7‰$ from the mean in coastal snow. The calculated $f_R \approx 35\%$, suggesting an important contribution of tropospheric sourced NO_3^- in the coastal snow. This estimation agrees fairly well with model simulations, considering both recycling of snow sourced NO_x (20–40% near the coast; Zatko et al., 2016) and tropospheric transport of mid-low latitude sourced NO_x (Lee et al., 2014). Thus, ice cores near the coast hold great potential to track past atmospheric NO_x/NO_3^- sources.

Considering the permanent sunlight during summertime in Antarctica, snow NO_3^- is expected to be mainly from the OH production channel ((R1) and (R5)) and global modeling agrees with this expectation (Alexander et al., 2009; Lee et al., 2014). On the coast, if the $\delta^{18}O(OH)$ values are close to those of $H_2O_{(v)}$ in the atmosphere, i.e., without large fractionation between OH and $H_2O_{(v)}$ (case 2A, Table 2), the range of $\delta^{18}O(OH)$, −28 to −47‰, seems to account for the x-intercept of the linear regression between $\delta^{18}O$ and $\Delta^{17}O$ of NO_3^- (−24‰; Fig. 4b). This is consistent with the expectation that the OH channel dominates NO_3^- production in summertime. Similar to the plateau results, if an additional fractionation between OH and $H_2O_{(v)}$ ($\varepsilon_{OH\text{-}H_2O}$) is taken into account (case 2B, Table 2), the $\delta^{18}O(OH)$ values (−77.6 to −95.7‰) are likely too negative to fit the observations.

Based on the f_R calculation above, the tropospheric sources in mid-low latitudes can contribute significantly to snow NO_3^-. For the oxygen isotopes, we must consider two cases: a) where NO_3^- is formed in the mid-low latitudes (i.e., oxidation takes place in the mid-low latitudes), and b) where NO_x is oxidized closer to the coast of Antarctica. For case a), considering that most of southern mid-low latitudes are open oceans and the sampling time is summer when dimethyl sulfide (DMS) levels are enhanced (Gabric et al., 2001; del Valle et al., 2009), we would expect the high end-member in Fig. 4b to be explained by NO_3^- formation with O_3 as the primary oxidant (e.g. (R7)–(R11)). The DMS and BrO pathways ((R7) and (R9)) produce the highest $\Delta^{17}O(NO_3^-)$ values, as the only oxidant is O_3 (Eq. (2)), and $\Delta^{17}O(NO_3^-)$ values produced by the two pathways are approximately equal. The OH channel (R5) produces the lowest $\Delta^{17}O(NO_3^-)$ values as $\Delta^{17}O(OH) \approx 0‰$, and N_2O_5 hydrolysis (R11) produces intermediate values ($\Delta^{17}O(NO_3^-) = 2/3\Delta^{17}O(NO_2) + 1/6\Delta^{17}O(O_3^*)$). An observed mean $\Delta^{17}O(NO_3^-)$ of 32 ± 2‰ in coastal snow corresponds to the contribution of the OH pathway of ≤30% (the maximum, ~30%, calculated assuming no contribution of N_2O_5 hydrolysis, see Case 2 in Table 2), suggesting a predominant role of BrO and/or DMS pathways in NO_3^- production. If the NO_3^- is mainly produced via either of these channels, the marine atmospheric NO_3^- in the mid-low latitudes should feature high $\Delta^{17}O$ values. However, the atmospheric $\Delta^{17}O(NO_3^-)$ mean in mid-low latitudes in the Indian Ocean sector is 25.1‰ (21.0–30.4‰; Table S1), much lower than $\Delta^{17}O$ values of NO_3^- calculated via the DMS or BrO pathways. In addition, the oxidation of NO_x by BrO in coastal East Antarctica has been suggested to be minor compared to the reaction with OH during summertime (Legrand et al., 2009; Kukui et al., 2012; Grilli et al., 2013). Lee et al. (2014) suggest that the degradation of PAN, a reservoir species of NO_x that is highly temperature sensitive, is a major source of NO_3^- to Antarctica. In this case (case b)), the oxygen isotopic composition of NO_3^- would be determined by high latitude oxidation. Even with this assumption, it is difficult to match the high observed coastal snow $\Delta^{17}O(NO_3^-)$. One possible explanation, for either case (a) or (b), is that $\Delta^{17}O(OH)$ is greatly underestimated. All of the existing $\Delta^{17}O(OH)$ values are from calculations (e.g., Morin et al., 2007; Savarino et al., 2016), with no environmental observations available thus far. A contradiction between expectations and observations of oxygen isotopes of NO_3^- was also observed at Summit, Greenland, and lack of understanding of isotopic composition of OH was proposed as a possible reason (Fibiger et al., 2016). However, given our results above, a high positive $\Delta^{17}O$ signal of OH seems unlikely due to the exchange of oxygen atoms with water in the atmosphere (Michalski et al., 2011). Another possibility is additional stratospheric input of NO_3^- and/or an underestimation of $\Delta^{17}O(O_3^*)$. If we take $\Delta^{17}O(O_3^*) \approx$ 52‰ (corresponding to $\Delta^{17}O \approx 35$‰ of bulk O_3, close to the result of laboratory experiments by Michalski et al. (2014)), the contribution of the OH pathway can be as much as or greater than 90%, consistent with expectations. Alternatively, if there are no systematic errors in the measurements of tropospheric O_3 using the nitrite coated filter technique ($\Delta^{17}O(O_3) \approx 26$‰) (Vicars et al., 2012; Vicars and Savarino, 2014), a stratospheric source with very high $\Delta^{17}O$ and/or an unknown NO_x chemistry is needed to explain the observed $\Delta^{17}O(NO_3^-)$ in the snow. A similar issue (underestimation of $\Delta^{17}O(NO_3^-)$) was also found for year round observations at Dome C (Savarino et al., 2016). Better constraint on the $\Delta^{17}O(O_3^*)$ in high latitudes is needed to resolve this and allow for interpretation of ice core NO_3^- records, even at the high-accumulation sites where most of the primary NO_3^- deposition information is preserved.

In summary, the summer coastal observations of $\delta^{15}N(NO_3^-)$ are best explained by a contribution from secondary NO_3^- via NO_x sourced from the plateau (~35%). Based upon modeling and our observations, the remaining fraction is likely best explained by tropospheric nitrogen sources (~65%), although a stratospheric source of NO_3^- cannot be ruled out. The oxygen isotopic composition of NO_3^-, both on the coast and the plateau, cannot be explained if OH exchanged with $H_2O_{(v)}$ in the atmosphere results in a large offset for $\delta^{18}O(OH)$ from $\delta^{18}O$ of $H_2O_{(v)}$. The formation of NO_3^- is expected to be dominated by $NO_2 + OH$ in summer, however, the isotopic observations require a high initial $\Delta^{17}O(O_3)$ (≈ 35‰ for bulk O_3) based on the current knowledge of NO_x chemistry and the oxygen isotopes of oxidants.

5. CONCLUSIONS

The purpose of this investigation was to track the differences in summertime NO_3^- atmospheric chemistry across the EAIS by means of the complete isotopic composition of NO_3^- in the snow and atmosphere. Concentration and isotopic compositions of NO_3^- in surface snow are dependent upon distance from the coast. On the plateau, snow NO_3^- is heavily influenced by post-depositional processing and local oxidation, confirming previous isotopic studies at Dome C and recent modeling studies that suggest significant release and recycling of snow-sourced NO_x. The production of secondary NO_3^- likely occurs both in the condensed phase (i.e., in the snow) and in the gas phase above the snowpack, based upon the isotopic composition of NO_3^- in the snow and in the atmosphere. During snow NO_3^- photolysis, some of the photoproducts are transported away, resulting in an enrichment of $\delta^{15}N(NO_3^-)$ in the snowpack and subsequently in the atmosphere. A mixing line between the NO_x oxidants O_3 and OH/H_2O can explain the linear relationship of $\delta^{18}O$ and $\Delta^{17}O$ of NO_3^- on the plateau, if there is no significant fractionation between OH and $H_2O_{(v)}$. A higher $\Delta^{17}O(O_3)$ value than observed predicts a better agreement between measured and expected $\Delta^{17}O(NO_3^-)$ values in the plateau snow.

From our observations, it is possible to estimate the contribution of secondary NO_3^- to coastal concentrations. In coastal snow, ~35% of NO_3^- is determined to be from snow-sourced NO_x from the interior (due to photolysis), while tropospheric transport from lower latitudes contributes about 65% to snow NO_3^-. The OH oxidation pathway plays an important role in gas phase NO_3^- production and, as on the plateau, the relationship between the oxygen isotopes of NO_3^- in coastal snow are best explained by $\delta^{18}O(OH) \approx \delta^{18}O(H_2O)_v$. However, the current knowledge on $\Delta^{17}O$ of oxidants and NO_x chemistry, and observations of mid-low latitude atmospheric NO_3^-, cannot account for the high observed snow $\Delta^{17}O(NO_3^-)$ values. Again, a high $\Delta^{17}O(O_3)$ (≈ 35‰) reconciles the discrepancies in observations and expectations, based upon chemical transport modeling, that tropospheric transport also contributes importantly to coastal deposition.

From both the plateau and coastal observations, it appears that ^{18}O fractionation for the equilibrium between OH and water vapor would be rather small or close to zero across the EAIS. Although the isotopic composition of O_3 has been analyzed recently at specific sites in Antarctica (e.g., Dome C; Savarino et al., 2016), further investigation is needed to determine the isotopes of OH and O_3 and/or the potential for missing NO_x chemistry. Coastal ice cores hold the best promise for reconstructing and tracking oxidant chemistry in the present and in the past via snow/ice core NO_3^-.

ACKNOWLEDGEMENTS

This research was supported by the National Science Foundation of China (Grant Nos. 41576190 and 41206188 to GS), the US National Science Foundation Antarctic Glaciology Program (Grant No. 1246223 to MGH), the Fundamental Research Funds for the Central Universities (to GS), and the National Key Research and Development Program of China (Grant No. 2016YFA0302204 to GS). The authors are grateful to Ruby Ho at Brown University and the 29th CHINARE inland members for technical support and assistance. The authors also would like to thank Prof. Jack J. Middelburg and two anonymous reviewers for their help in the development and improvement of this paper.

APPENDIX A. SUPPLEMENTARY MATERIAL

Supplementary data associated with this article can be found, in the online version, at https://doi.org/10.1016/j.gca.2018.03.025.

REFERENCES

Alexander B., Hastings M., Allman D., Dachs J., Thornton J. and Kunasek S. (2009) Quantifying atmospheric nitrate formation pathways based on a global model of the oxygen isotopic composition ($\Delta^{17}O$) of atmospheric nitrate. *Atmos. Chem. Phys.* **9**, 5043–5056.

Berhanu T. A., Meusinger C., Erbland J., Jost R., Bhattacharya S., Johnson M. S. and Savarino J. (2014) Laboratory study of nitrate photolysis in Antarctic snow. II. Isotopic effects and wavelength dependence. *J. Chem. Phys.* **140**, 244306.

Berhanu T. A., Savarino J., Erbland J., Vicars W. C., Preunkert S., Martins J. F. and Johnson M. S. (2015) Isotopic effects of nitrate photochemistry in snow: a field study at Dome C, Antarctica. *Atmos. Chem. Phys.* **15**, 11243–11256.

Bertler N., Mayewski P. A., Aristarain A., Barrett P., Becagli S., Bernardo R., Bo S., Xiao C., Curran M. and Qin D. (2005) Snow chemistry across Antarctica. *Ann. Glaciol.* **41**, 167–179.

Bloss W., Lee J., Heard D., Salmon R. A., Bauguitte S.-B., Roscoe H. and Jones A. (2007) Observations of OH and HO_2 radicals in coastal Antarctica. *Atmos. Chem. Phys.* **7**, 4171–4185.

Blunier T., Floch G., Jacobi H.-W. and Quansah E. (2005) Isotopic view on nitrate loss in Antarctic surface snow. *Geophys. Res. Lett.* **32**, L13501.

Bock J., Savarino J. and Picard G. (2016) Air–snow exchange of nitrate: a modelling approach to investigate physicochemical processes in surface snow at Dome C, Antarctica. *Atmos. Chem. Phys.* **16**, 12531–12550.

Buffen A. M., Hastings M. G., Thompson L. G. and Mosley-Thompson E. (2014) Investigating the preservation of nitrate isotopic composition in a tropical ice core from the Quelccaya Ice Cap, Peru. *J. Geophys. Res.* **119**, 2674–2697.

Casado M., Landais A., Massondelmotte V., Genthon C., Kerstel E., Kassi S., Arnaud L., Picard G., Prie F. and Cattani O. (2016) Continuous measurements of isotopic composition of water vapour on the East Antarctic Plateau. *Atmos. Chem. Phys.* **16**, 1–26.

Casciotti K., Sigman D., Hastings M. G., Böhlke J. and Hilkert A. (2002) Measurement of the oxygen isotopic composition of nitrate in seawater and freshwater using the denitrifier method. *Anal. Chem.* **74**, 4905–4912.

Chen G., Davis D., Crawford J., Nowak J. B., Eisele F., Iii R. L. M., Tanner D., Buhr M., Shetter R. and Lefer B. (2001) An investigation of South Pole HOx chemistry: comparison of model results with ISCAT observations. *Geophys. Res. Lett.* **28**, 3633–3636.

Das I., Bell R. E., Scambos T. A., Wolovick M., Creyts T. T., Studinger M., Frearson N., Nicolas J. P., Lenaerts J. T. and van den Broeke M. R. (2013) Influence of persistent wind scour on the surface mass balance of Antarctica. *Nat. Geosci.* **6**, 367–371.

Davis D., Chen G., Buhr M., Crawford J., Lenschow D., Lefer B., Shetter R., Eisele F., Mauldin L. and Hogan A. (2004) South Pole NO_x chemistry: an assessment of factors controlling variability and absolute levels. *Atmos. Environ.* **38**, 5375–5388.

Davis D. D., Seelig J., Huey G., Crawford J., Chen G., Wang Y., Buhr M., Helmig D., Neff W., Blake D., Arimot R. and Eisele F. (2008) A reassessment of Antarctic plateau reactive nitrogen based on ANTCI 2003 airborne and ground based measurements. *Atmos. Environ.* **42**, 2831–2848.

del Valle D. A., Kieber D. J., Toole D. A., Brinkley J. and Kiene R. P. (2009) Biological consumption of dimethylsulfide (DMS) and its importance in DMS dynamics in the Ross Sea, Antarctica. *Limnol. Oceanogr.* **54**, 785–798.

Ding M., Xiao C., Li Y., Ren J., Hou S., Jin B. and Sun B. (2011) Spatial variability of surface mass balance along a traverse route from Zhongshan station to Dome A, Antarctica. *J. Glaciol.* **57**, 658–666.

Dubey M. K., Mohrschladt R., Donahue N. M. and Anderson J. G. (1997) Isotope specific kinetics of hydroxyl radical (OH) with water (H_2O): testing models of reactivity and atmospheric fractionation. *J. Phys. Chem.* **101**, 1494–1500.

Erbland J., Savarino J., Morin S., France J. L., Frey M. M. and King M. D. (2015) Air-snow transfer of nitrate on the East Antarctic plateau – Part 2: An isotopic model for the interpretation of deep ice-core records. *Atmos. Chem. Phys.* **15**, 12079–12113.

Erbland J., Vicars W., Savarino J., Morin S., Frey M., Frosini D., Vince E. and Martins J. (2013) Air-snow transfer of nitrate on the East Antarctic Plateau – Part 1: Isotopic evidence for a photolytically driven dynamic equilibrium in summer. *Atmos. Chem. Phys.* **13**, 6403–6419.

Fibiger D. L., Dibb J. E., Chen D., Thomas J. L., Burkhart J. F., Huey L. G. and Hastings M. G. (2016) Analysis of nitrate in the snow and atmosphere at Summit, Greenland: chemistry and transport. *J. Geophys. Res.* **121**, 5010–5030.

Fibiger D. L., Hastings M. G., Dibb J. E. and Huey L. G. (2013) The preservation of atmospheric nitrate in snow at Summit, Greenland. *Geophys. Res. Lett.* **40**, 3484–3489.

Frey M., Roscoe H., Kukui A., Savarino J., France J., King M., Legrand M. and Preunkert S. (2015) Atmospheric nitrogen oxides (NO and NO_2) at Dome C, East Antarctica, during the OPALE campaign. *Atmos. Chem. Phys.* **15**, 7859–7875.

Frey M. M., Savarino J., Morin S., Erbland J. and Martins J. (2009) Photolysis imprint in the nitrate stable isotope signal in snow and atmosphere of East Antarctica and implications for reactive nitrogen cycling. *Atmos. Chem. Phys.* **9**, 8681–8696.

Freyer H. D., Kobel K., Delmas R. J., Kley D. and Legrand M. R. (1996) First results of $^{15}N/^{14}N$ ratios in nitrate from alpine and polar ice cores. *Tellus B* **48**, 93–105.

Gabric A. J., Whetton P. H. and Cropp R. (2001) Dimethylsulphide production in the subantarctic Southern Ocean under enhanced greenhouse conditions. *Tellus B* **53**, 273–287.

Grannas A., Jones A. E., Dibb J., Ammann M., Anastasio C., Beine H., Bergin M., Bottenheim J., Boxe C. and Carver G. (2007) An overview of snow photochemistry: evidence, mechanisms and impacts. *Atmos. Chem. Phys.* **7**, 4329–4373.

Grilli R., Legrand M., Kukui A., Méjean G., Preunkert S. and Romanini D. (2013) First investigations of IO, BrO, and NO_2 summer atmospheric levels at a coastal East Antarctic site using mode-locked cavity enhanced absorption spectroscopy. *Geophys. Res. Lett.* **40**, 791–796.

Hastings M. G., Jarvis J. C. and Steig E. J. (2009) Anthropogenic impacts on nitrogen isotopes of ice-core nitrate. *Science* **324**, 1288, 1288-1288.

Hastings M. G., Sigman D. M. and Steig E. J. (2005) Glacial/interglacial changes in the isotopes of nitrate from the Greenland Ice Sheet Project 2 (GISP2) ice core. *Glob. Biogeochem. Cycl.* **19**, GB4024.

Hoering T. (1960) The isotopic composition of the ammonia and the nitrate ion in rain. *Geochim. Cosmochim. Acta* **12**, 97–102.

Hoffmann G. (1995) *Stabile Wasserisotope im allgemeinen Zirkulationsmodell ECHAM*. Universität Hamburg, Hamburg, p. 98.

Hou S., Li Y., Xiao C., Pang H. and Xu J. (2009) Preliminary results of the close-off depth and the stable isotopic records along a 109.91 m ice core from Dome A, Antarctica. *Sci. China Ser. D* **52**, 1502–1509.

Jacobi H.-W., Annor T. and Quansah E. (2006) Investigation of the photochemical decomposition of nitrate, hydrogen peroxide, and formaldehyde in artificial snow. *J. Photochem. Photobiol. A* **179**, 330–338.

Jacobi H.-W. and Hilker B. (2007) A mechanism for the photochemical transformation of nitrate in snow. *J. Photochem. Photobiol. A* **185**, 371–382.

Johnsen S. J., Clausen H. B., Dansgaard W., Gundestrup N. S., Hammer C. U., Andersen U., Andersen K. K., Hvidberg C. S., Dahl-Jensen D. and Steffensen J. P. (1997) The $\delta^{18}O$ record along the Greenland Ice Core Project deep ice core and the problem of possible Eemian climatic instability. *J. Geophys. Res.* **102**, 26397–26410.

Kaiser J., Hastings M. G., Houlton B. Z., Röckmann T. and Sigman D. M. (2007) Triple oxygen isotope analysis of nitrate using the denitrifier method and thermal decomposition of N_2O. *Anal. Chem.* **79**, 599–607.

Krankowsky D., Lämmerzahl P., Mauersberger K., Janssen C., Tuzson B. and Röckmann T. (2007) Stratospheric ozone isotope fractionations derived from collected samples. *J. Geophys. Res.* **112**, 271–283.

Kukui A., Legr M., Ancellet G., Gros V., Bekki S., Sarda-Estève R., Loisil R. and Preunkert S. (2012) Measurements of OH and RO2 radicals at the coastal Antarctic site of Dumont d'Urville (East Antarctica) in summer 2010–2011. *J. Geophys. Res.* **117**, 12310.

Kukui A., Legrand M., Preunkert S., Frey M., Loisil R., Gil Roca J., Jourdain B., King M., France J. and Ancellet G. (2014) Measurements of OH and RO_2 radicals at Dome C, East Antarctica. *Atmos. Chem. Phys.* **14**, 12373–12392.

Kunasek S., Alexander B., Steig E., Hastings M., Gleason D. and Jarvis J. (2008) Measurements and modeling of $\Delta^{17}O$ of nitrate in snowpits from Summit, Greenland. *J. Geophys. Res.* **113**, D24302.

Lee H.-M., Henze D. K., Alexander B. and Murray L. T. (2014) Investigating the sensitivity of surface-level nitrate seasonality in Antarctica to primary sources using a global model. *Atmos. Environ.* **89**, 757–767.

Legrand M. and Delmas R. (1986) Relative contributions of tropospheric and stratospheric sources to nitrate in Antarctic snow. *Tellus B* **38**, 236–249.

Legrand M., Preunkert S., Jourdain B., Gallée H., Goutail F., Weller R. and Savarino J. (2009) Year-round record of surface ozone at coastal (Dumont d'Urville) and inland (Concordia) sites in East Antarctica. *J. Geophys. Res.* **114**, D20306.

Mauersberger K., Krankowsky D. and Janssen C. (2003) Oxygen isotope processes and transfer reactions. *Space Sci. Rev.* **106**, 265–279.

Mauldin R. L., Eisele F. L., Tanner D. J., Kosciuch E., Shetter R., Lefer B., Hall S. R., Nowak J. B., Buhr M., Chen G., Wang P. and Davis D. (2001) Measurements of OH, H_2SO_4, and MSA at the South Pole during ISCAT. *Geophys. Res. Lett.* **28**, 3629–3632.

McCabe J., Boxe C., Colussi A., Hoffmann M. and Thiemens M. (2005) Oxygen isotopic fractionation in the photochemistry of nitrate in water and ice. *J. Geophys. Res.* **110**, D15310.

McCabe J. R., Thiemens M. H. and Savarino J. (2007) A record of ozone variability in South Pole Antarctic snow: role of nitrate oxygen isotopes. *J. Geophys. Res.* **112**, D12303.

Michalski G., Böhlke J. K. and Thiemens M. (2004) Long term atmospheric deposition as the source of nitrate and other salts in the Atacama Desert, Chile: new evidence from mass-independent oxygen isotopic compositions. *Geochim. Cosmochim. Acta* **68**, 4023–4038.

Michalski G., Bhattacharya S. and Mase D. F. (2011) Oxygen isotope dynamics of atmospheric nitrate and its precursor molecules. In *Handbook of Environmental Isotope Geochemistry* (ed. M. Baskaran). Springer, Berlin, pp. 613–635.

Michalski G., Bhattacharya S. K. and Girsch G. (2014) NOx cycle and tropospheric ozone isotope anomaly: an experimental investigation. *Atmos. Chem. Phys.* **14**, 9443–9483.

Michalski G., Scott Z., Kabiling M. and Thiemens M. H. (2003) First measurements and modeling of $\Delta^{17}O$ in atmospheric nitrate. *Geophys. Res. Lett.* **30**, 1870.

Moore H. (1974) Isotopic measurement of atmospheric nitrogen compounds. *Tellus* **26**, 169–174.

Morin S., Savarino J., Bekki S., Gong S. and Bottenheim J. (2007) Signature of Arctic surface ozone depletion events in the isotope anomaly ($\Delta^{17}O$) of atmospheric nitrate. *Atmos. Chem. Phys.* **7**, 1451–1469.

Morin S., Savarino J., Frey M. M., Domine F., Jacobi H.-W., Kaleschke L. and Martins J. M. (2009) Comprehensive isotopic composition of atmospheric nitrate in the Atlantic Ocean boundary layer from 65 S to 79 N. *J. Geophys. Res.* **114**.

Murray L. T., Jacob D. J., Logan J. A., Hudman R. C. and Koshak W. J. (2012) Optimized regional and interannual variability of lightning in a global chemical transport model constrained by LIS/OTD satellite data. *J. Geophys. Res.* **117**, D20307.

Röthlisberger R., Hutterli M. A., Wolff E. W., Mulvaney R., Fischer H., Bigler M., Goto-Azuma K., Hansson M. E., Ruth U. and Siggaard-Andersen M.-L. (2002) Nitrate in Greenland and Antarctic ice cores: a detailed description of post-depositional processes. *Ann. Glaciol.* **35**, 209–216.

Savarino J., Bhattacharya S. K., Morin S., Baroni M. and Doussin J. F. (2008) The NO+O_3 reaction: a triple oxygen isotope perspective on the reaction dynamics and atmospheric implications for the transfer of the ozone isotope anomaly. *J. Chem. Phys.* **128**, 194303.

Savarino J., Kaiser J., Morin S., Sigman D. M. and Thiemens M. H. (2007) Nitrogen and oxygen isotopic constraints on the origin of atmospheric nitrate in coastal Antarctica. *Atmos. Chem. Phys.* **7**, 1925–1945.

Savarino J., Vicars W. C., Legrand M., Preunkert S., Jourdain B., Frey M. M., Kukui A., Caillon N. and Gil Roca J. (2016) Oxygen isotope mass balance of atmospheric nitrate at Dome C, East Antarctica, during the OPALE campaign. *Atmos. Chem. Phys.* **16**, 2659–2673.

Shi G., Buffen A. M., Hastings M. G., Li C., Ma H., Li Y., Sun B., An C. and Jiang S. (2015) Investigation of post-depositional processing of nitrate in East Antarctic snow: isotopic constraints on photolytic loss, re-oxidation, and source inputs. *Atmos. Chem. Phys.* **15**, 9435–9453.

Shi G., Hastings M. G., Yu J., Ma T., Hu Z., An C., Li C., Ma H., Jiang S. and Li Y. (2018) Nitrate deposition and preservation in the snowpack along a traverse from coast to the ice sheet summit (Dome A) in East Antarctica. *Cryosphere* **12**, 1177–1194.

Shi G., Li Y., Jiang S., An C., Ma H., Sun B. and Wang Y. (2012) Large-scale spatial variability of major ions in the atmospheric wet deposition along the China Antarctica transect (31°N∼69°S). *Tellus B* **64**, 17134.

Sigman D. M., Casciotti K. L., Andreani M., Barford C., Galanter M. and Böhlke J. K. (2001) A bacterial method for the nitrogen isotopic analysis of nitrate in seawater and freshwater. *Anal. Chem.* **73**, 4145–4153.

Slusher D. L., Neff W. D., Kim S., Huey L. G., Wang Y., Zeng T., Tanner D. J., Blake D. R., Beyersdorf A. and Lefer B. L. (2010) Atmospheric chemistry results from the ANTCI 2005 Antarctic plateau airborne study. *J. Geophys. Res.* **115**, D07304.

Traversi R., Becagli S., Brogioni M., Caiazzo L., Ciardini V., Giardi F., Legrand M., Macelloni G., Petkov B., Preunkert S., Scarchilli C., Severi M., Vitale V. and Udisti R. (2017) Multi-year record of atmospheric and snow surface nitrate in the central Antarctic plateau. *Chemosphere* **172**, 341–354.

Traversi R., Becagli S., Castellano E., Largiuni O., Migliori A., Severi M., Frezzotti M. and Udisti R. (2004) Spatial and temporal distribution of environmental markers from Coastal to Plateau areas in Antarctica by firn core chemical analysis. *Int. J. Environ. Anal. Chem.* **84**, 457–470.

Traversi R., Usoskin I., Solanki S., Becagli S., Frezzotti M., Severi M., Stenni B. and Udisti R. (2012) Nitrate in polar ice: a new tracer of solar variability. *Sol. Phys.* **280**, 237–254.

Udisti R., Becagli S., Benassai S., Castellano E., Fattori I., Innocenti M., Migliori A. and Traversi R. (2004) Atmosphere-snow interaction by a comparison between aerosol and uppermost snow-layers composition at Dome C, East Antarctica. *Ann. Glaciol.* **39**, 53–61.

Vicars W. C., Bhattacharya S., Erbland J. and Savarino J. (2012) Measurement of the 17O-excess (Δ^{17}O) of tropospheric ozone using a nitrite-coated filter. *Rapid Commun. Mass. Spectrom.* **26**, 1219–1231.

Vicars W. C. and Savarino J. (2014) Quantitative constraints on the ^{17}O-excess (Δ^{17}O) signature of surface ozone: ambient measurements from 50°N to 50°S using the nitrite-coated filter technique. *Geochim. Cosmochim. Acta* **135**, 270–287.

Wagenbach D., Legrand M., Fischer H., Pichlmayer F. and Wolff E. W. (1998) Atmospheric near-surface nitrate at coastal Antarctic sites. *J. Geophys. Res.* **103**, 11007–11020.

Weller R., Traufetter F., Fischer H., Oerter H., Piel C. and Miller H. (2004) Postdepositional losses of methane sulfonate, nitrate, and chloride at the European Project for Ice Coring in Antarctica deep-drilling site in Dronning Maud Land, Antarctica. *J. Geophys. Res.* **109**, D07301.

Xu G. and Gao Y. (2015) Characterization of marine aerosols and precipitation through shipboard observations on the transect between 31°N–32°S in the West Pacific. *Atmos. Pollut. Res.* **6**, 154–161.

Xu G., Gao Y., Lin Q., Li W. and Chen L. (2013) Characteristics of water-soluble inorganic and organic ions in aerosols over the Southern Ocean and coastal East Antarctica during austral summer. *J. Geophys. Res.* **118**(13), 303–313, 318.

Yu Z. and Elliott E. M. (2017) Novel method for nitrogen isotopic analysis of soil-emitted nitric oxide. *Environ. Sci. Technol.* **51**, 6268–6278.

Zatko M., Grenfell T., Alexander B., Doherty S., Thomas J. and Yang X. (2013) The influence of snow grain size and impurities on the vertical profiles of actinic flux and associated NO_x emissions on the Antarctic and Greenland ice sheets. *Atmos. Chem. Phys.* **13**, 3547–3567.

Zatko M. C., Geng L., Alexander B., Sofen E. D. and Klein K. (2016) The impact of snow nitrate photolysis on boundary layer chemistry and the recycling and redistribution of reactive nitrogen across Antarctica and Greenland in a global chemical transport model. *Atmos. Chem. Phys.* **16**, 2819–2842.

Associate editor: Jack J. Middelburg